Supporting information

Tautomerism and Nucleophilic Addition Influenced Performance on Aqueous Organic Redox Flow Batteries of Chelidamic Acid and Chelidonic Acid

Surya Prakash,[a] Alagar Ramar,[a] Fu-Ming Wang,[a,b,c,d]* Kefyalew Wagari Guji,[a] Citra Deliana Dewi Sundari,[e] and Laurien Merinda[a]

[a]Graduate Institute of Applied Science and Technology, National Taiwan University of Science and Technology, No.43, Sec. 4, Keelung Road, Taipei 106, Taiwan, R.O.C.
[b]R&D Center for Membrane Technology, Chung Yuan Christian University, Taoyuan, Taiwan
[c]Sustainable Energy Center, National Taiwan University of Science and Technology, Taipei, Taiwan
[d]Department of Chemical Engineering, Chung Yuan Christian University, Taoyuan, Taiwan
[e]Department of Chemistry Education, UIN Sunan Gunung Djati Bandung, Bandung, Indonesia

*Corresponding author, TEL: +886 2 27303755; FAX: +886 2 27303733 (Prof. Fu-Ming Wang)
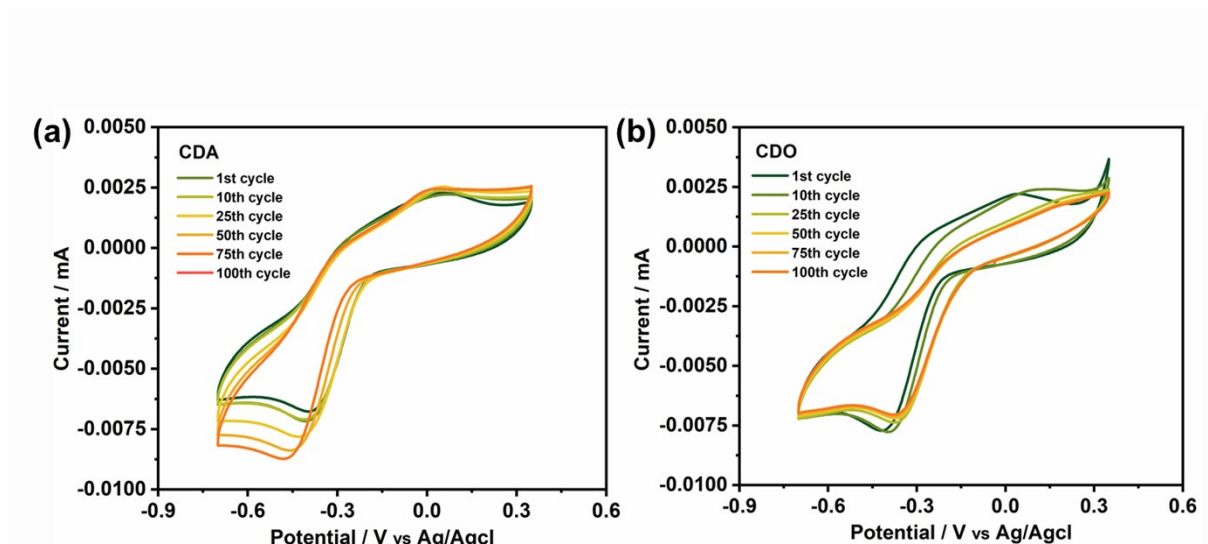E-mail address: mccabe@mail.ntust.edu.tw (Prof. Fu-Ming Wang)

Fig. S1 Cyclic voltammetry of 5 mM of (a) CDA and (b) CDO at the scan rate of 10 mV/s in 1 M KOH supporting solution.
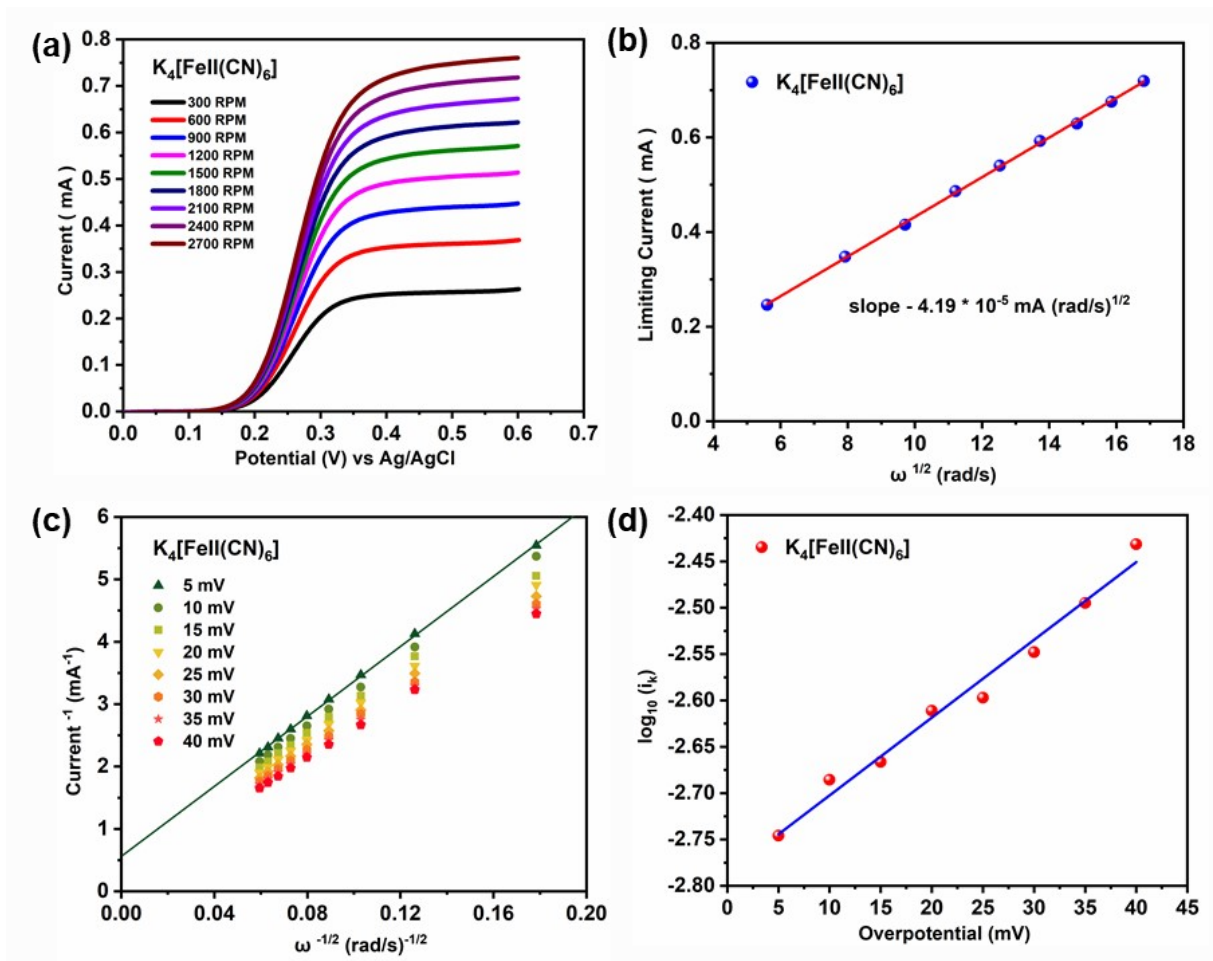
Fig. S2 (a) The linear sweep voltammetry of 5 mM of $K_4[Fe^{II}(CN)_6]$ at 10 mV/s scan rate in 1 M KOH supporting electrolyte using RDE (b) levinch plot ω ½ against limiting current to calculate the D value of $K_4[Fe^{II}(CN)_6]$ (D - 6.15 × 10^{-6} cm^2 s^{-1}) (c) levinch plot of $K_4[Fe^{II}(CN)_6]$ derived from (a), (d) Tafel plot of $K_4[Fe^{II}(CN)_6]$ derived from (c) to find the kinetic rate constant k$_0$- 5.93 × 10^{-2} cm^2 s^{-1}.
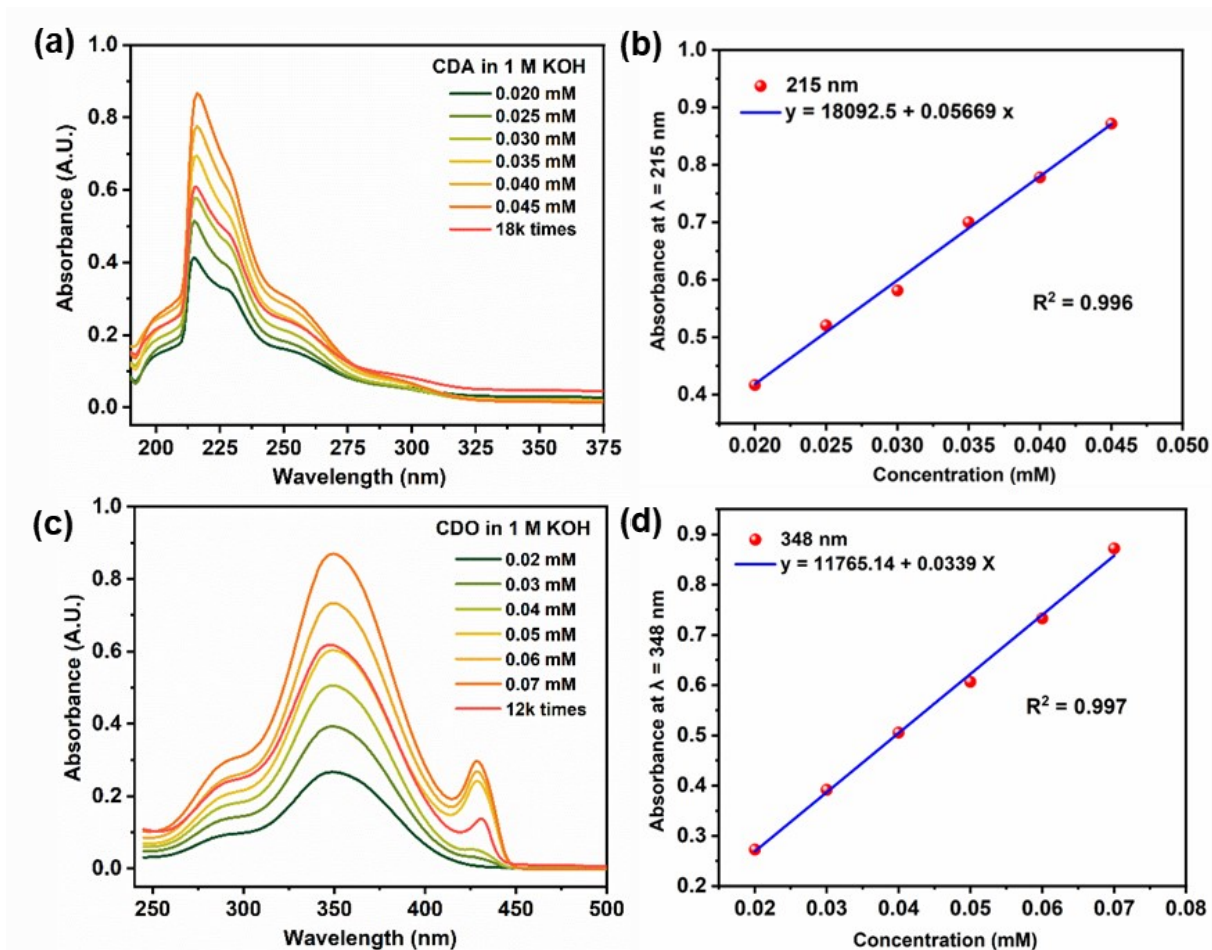
Fig. S3 (a,c) shows the UV-vis spectra of CDA and CDO at various Concentration, the red line indicates saturated CDA and CDO solutions diluted to 18 k and 12k times in 1 M KOH (b) shows the absorbance peak of different concentrations of CDA at 215 nm (d) illustrate the absorbance peak of different concentrations of CDO at 348 nm.
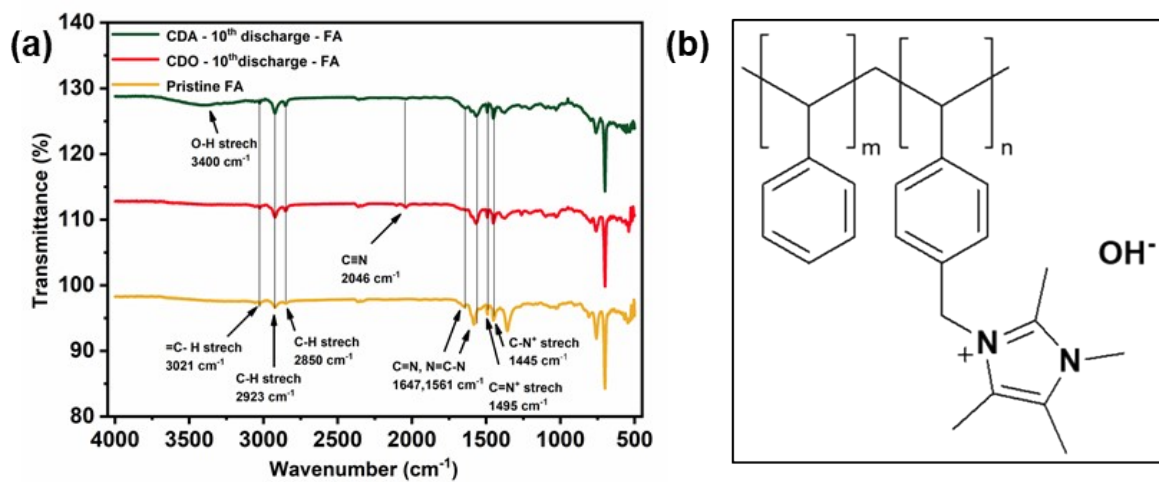
Fig. S4 (a) shows FTIR spectra of the pristine X-37 FA membrane and the X-37 FA membrane after 10 cycles of CDO and CDA (b) displays the chemical structure of the X-37 FA membrane.
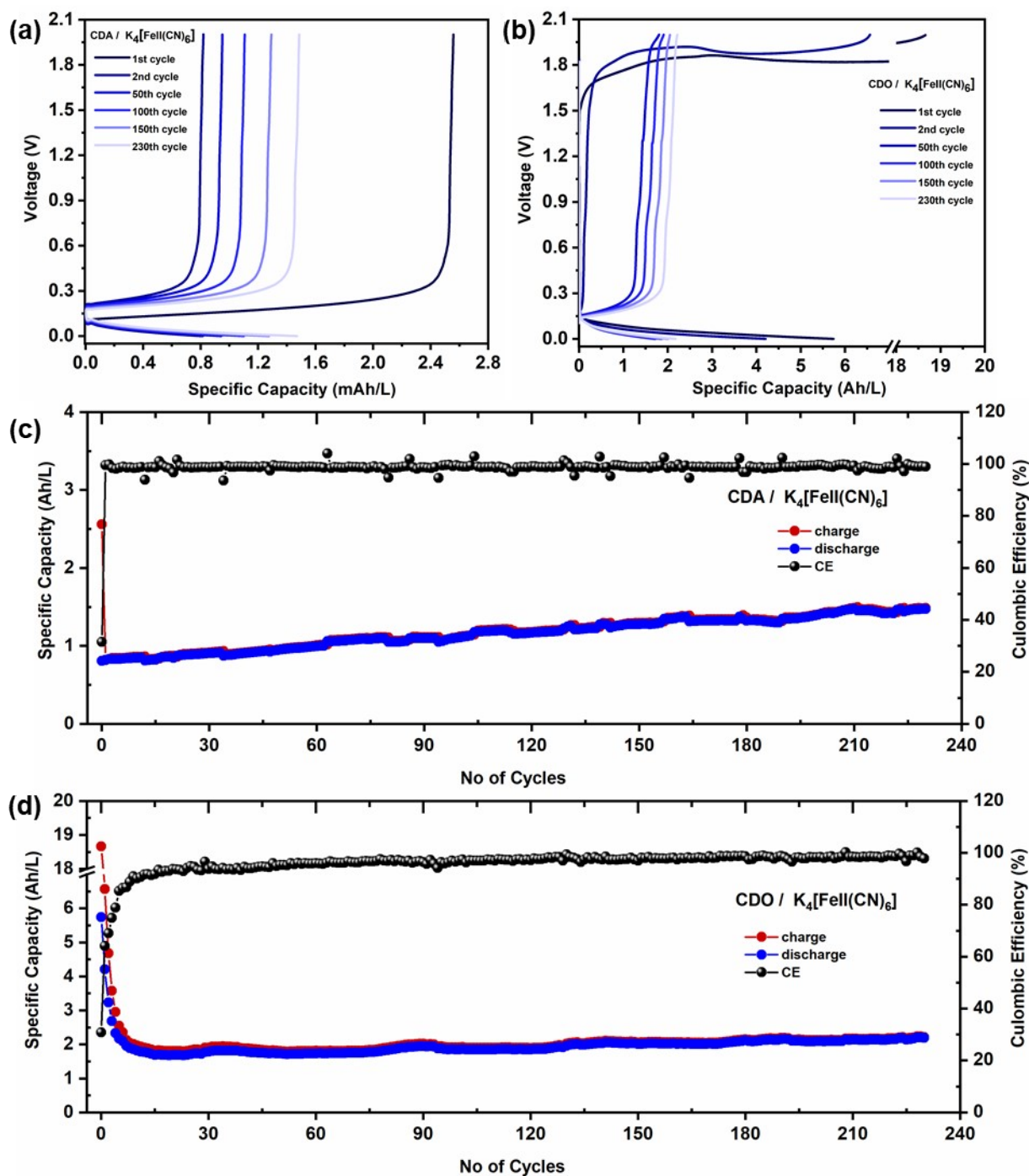
Fig. S5 shows the ARFB results of (a, b) charge-discharge profile of CDA and CDO (c, d) no of cycles vs charge, discharge capacity and CE of CDA and CDO (The capacity-limiting side contains 25 ml of 0.4 M CDA/CDO, while the non-capacity-limiting side contains 50 ml of 0.4 M $K_4[Fe^{II}(CN)_6]$ in 1 M KOH. The solutions are circulated through the flow cell at 80 rpm, with a current density of 40 mA/cm² applied for analysis within a voltage range of 0-2 V)

Fig. S6 shows the ARFB results of (a, b) cycle number vs CE, EE, and VE of CDA and CDO (The capacity-limiting side contains 25 ml of 0.4 M CDA/CDO, while the non-capacity-limiting side contains 50 ml of 0.4 M $K_4[Fe^{II}(CN)_6]$ in 1 M KOH. The solutions are circulated through the flow cell at 80 rpm, with a current density of 40 mA/cm² applied for analysis within a voltage range of 0-2 V)
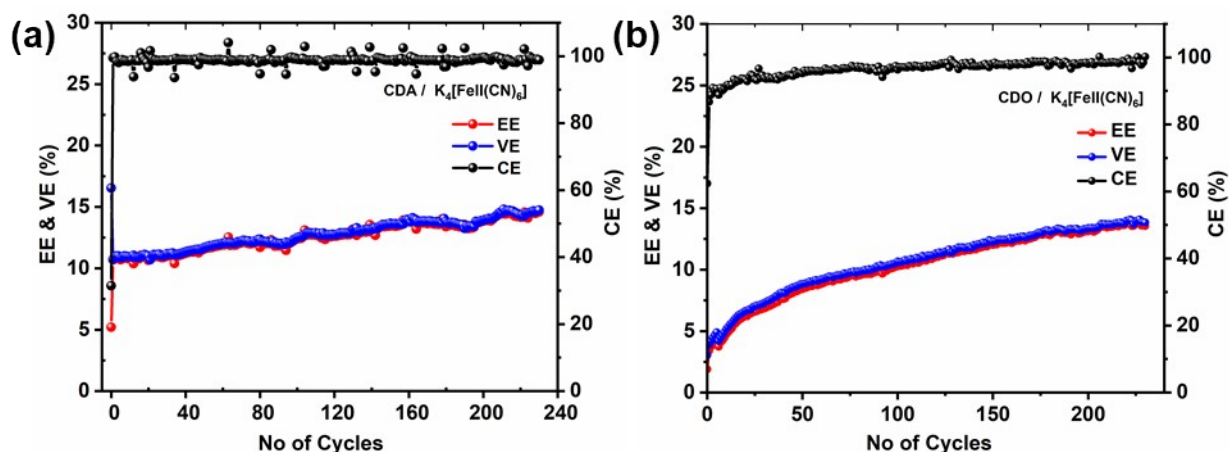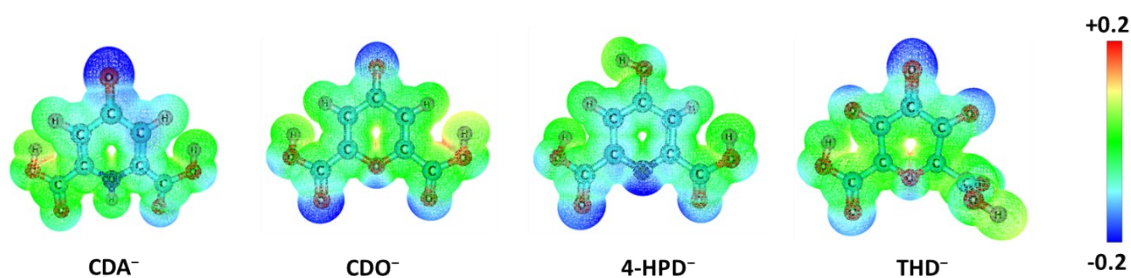

Fig. S7 Shows the molecular charge distribution of CDA, CDO, 4-HPD⁻ and THD⁻.
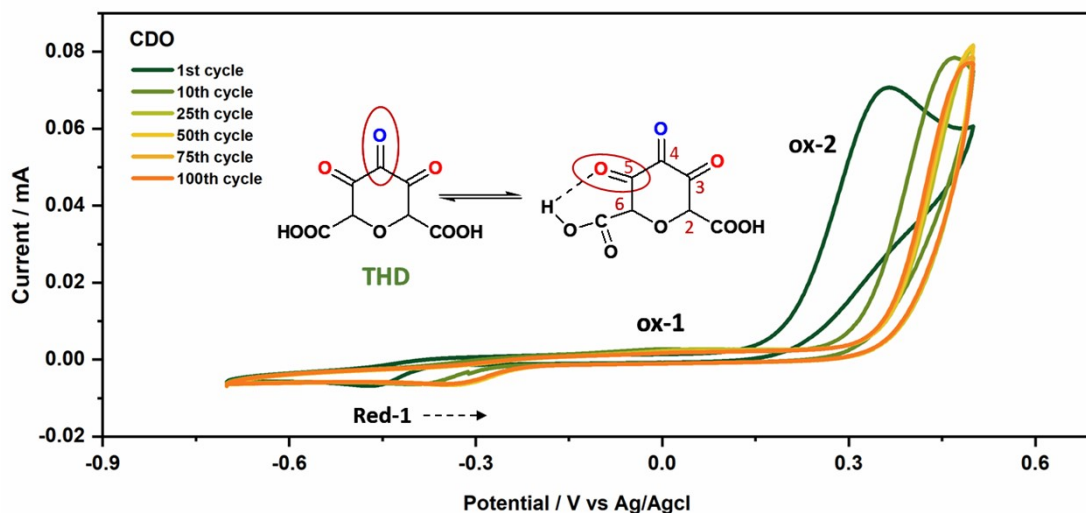
Fig. S8 Cyclic voltammetry of 5 mM CDO at a scan rate of 10 mV/s in a 1 M KOH supporting solution, along with a schematic representation of the H-bonded THD, highlighting the activated carbonyl group indicated by a red circle. The reversibility of the CV was analyzed over a potential range from -0.7 V to 0.5 V, revealing two oxidation peaks close to 0 V and 0.37 V. The first oxidation peak near 0 V is attributed to the carbonyl group at the 4th position, which degrades within 10 cycles (Fig. S1). The second oxidation peak at 0.37 V is associated with two α-carbonyl groups, with the α-carbonyl group at the 5th position being particularly involved in the redox reaction. This involvement is supported by evidence of intermolecular hydrogen bonding and further confirmed by DFT analysis (Fig.S7). The intermolecular hydrogen bonding activates the carbonyl group, which leads to the redox process. The reduction process involves a one-electron transfer that occurs after 10 cycles.[1] These observed peak shifting in the CV, along with the resulting degradation, are directly related to the of capacity deterioration at the beginning of the charge-discharge cycles, as shown in Fig. 2 and S5.

Reference

1.   C. Mirle, V. Medabalmi and K. Ramanujam, *Catal. Today*, 2021, **370**, 173-180.